Generation of abnormal acoustic noise: Singing of a cavitating tip vortex

Xiaoxing Peng,[1] Benlong Wang,[2,3,4,*] Haoyu Li,[2] Lianghao Xu,[1] and Mingtai Song[1]
[1]*National Key Laboratory on Ship Vibration & Noise, China Ship Scientific Research Center, Wuxi 214082, China*
[2]*Department of Engineering Mechanics, Shanghai Jiao Tong University, Shanghai 200240, China*
[3]*MOE Key Laboratory of Hydrodynamics, Shanghai Jiao Tong University, Shanghai 200240, China*
[4]*Collaborative Innovation Center for Advanced Ship and Deep-Sea Exploration, Shanghai 200240, China*
(Received 14 January 2017; published 15 May 2017)

We present experimental results and a theoretical analysis for the singing of a cavitating tip vortex (SCTV), which has been occasionally observed under special conditions in a few experimental facilities around the world since the 1990s. Due to lack of repeatability, little is known about the generation mechanism of SCTV [R. E. A. Arndt, Annu. Rev. Fluid Mech. **34**, 143 (2002)]. In the present work we propose an experimental procedure to produce the SCTV phenomenon at selected flow conditions in the China Ship Scientific Research Center cavitation mechanism tunnel. By analyzing the frequency characteristics of the acoustical signal and the bubble dynamics, it is found that the tone of SCTV matches the natural frequency of radial oscillation of the cylinder bubble and a formulation to predict SCTV is developed. Good agreement is obtained between the proposed formulation and the experimental data from different facilities.

DOI: 10.1103/PhysRevFluids.2.053602

I. INTRODUCTION

Various tip vortices occur in both aerodynamic and hydrodynamic circumstances [1–3]. In particular, tip vortex cavitation is often found in marine propellers and turbines due to the remarkable drop in local pressure and the phase transition between liquid water and vapor. Singing of a cavitating tip vortex (SCTV), named by Maines and Arndt [4], is a special phenomenon in which abnormal acoustic noise at a particular frequency is emitted due to tip vortex cavitation. It has been thought for a long time that this phenomenon occurs over a very narrow range of cavitation numbers and it has been occasionally observed under a few special conditions in the past few decades [5,6]. A standing wave was also believed to be the reason for SCTV and it occurs over a very narrow range of cavitation numbers [4]. The basis of this speculation is that a standing wave is possible in hollow swirling water jets [7] and uniform axial flow [8].

Thus far, due to the lack of systematic experimental data as proof, detailed analysis and experimental verification of the generation mechanism are not possible. Therefore, the physical mechanism of this phenomenon is still not clear [2]. A more recent attempt to analyze the problem was the work of Pennings *et al.*, who derived a theoretical formulation to predict the occurrence of vortex singing using compressible flow theory [9]. According to the dispersion relationship and experimental results, zero group velocity was postulated to be the source of resonance, which put researchers one step closer to discovering SCTV. Unfortunately, no SCTV phenomenon was captured in their experiments. To further investigate SCTV under controllable flow parameters, a combination of experimental measurements and theoretical analysis is carried out in the present work to give an in depth understanding of the generation mechanism of SCTV.

*benlongwang@sjtu.edu.cn

II. EXPERIMENTAL RESULTS

Experiments have been conducted in the cavitation mechanism tunnel of China Ship Scientific Research Center (CSSRC) with a square cross section of $225 \times 225\ \mathrm{mm}^2$. There is a large degassing tank installed in the downstream of the test section to control the air content of the water. In the present experiments, the air content of the incoming water is 0.77 times the saturated air concentration. An elliptic hydrofoil of section NACA 66_2-415 is used as the test model with a maximum chord of 94.2 mm and a half span of 112.5 mm. The model is installed in the horizontal center of the test section with the tip in the centerline of the test section and the attack angle is 7°. To visualize the development of tip vortex cavitation, a Photron APX high-speed video camera with 2000 frames/s (fps) is used and a light-emitting diode lamp is used as the light source. Both of these devices are set in the bottom of the test section. One B&K 8103 hydrophone is installed in the side window of the water tunnel with a container filled with water.

By trial and error, reliable experimental techniques and procedures were developed to produce repeatable and controllable SCTV, which had not been achieved before. During the experiments, strong tip vortex cavitations were first generated at expected flow speeds W_∞ and much lower cavitation number by decreasing the pressure P_∞. In the case of cavitation numbers lower than the desired one, the tip vortex cavity looks stationary and the size is quite thick. As we gradually increase the background pressure of the water tunnel (i.e., the cavitation number), the radius of the cavitating tip vortex decreases. At each background pressure, we must wait for a few minutes to let the flow pattern fully develop, which is particularly important for the success of producing SCTV. During the pressure-decreasing process, vortex singing often occurs before desinence of cavitation. In the case of vortex singing, the form of vortex cavitation will be unstable and go through three different states as shown in Fig. 1.

Before singing, the cavitating vortex tube resembles the same pattern as that at low cavitation number and the attached sheet cavity around the surface of the hydrofoil tip is stable, as shown in Fig. 1(a). The corresponding acoustic records are in recording SM.1 in [10]. After a while, the cavitating vortex tube starts to expand and contract in synchronicity with the attached sheet cavity, as shown in Fig. 1(b). Simultaneously, abnormal sound can be heard by the naked ear. The corresponding acoustic recording is in recording SM.2 in [10]. This process can continue for a few minutes. Then the singing disappears suddenly; meanwhile, the attached sheet cavity vanishes and the diameter of the cavitating vortex tube decreases dramatically, as shown in Fig. 1(c).

Acoustic measurement is a more direct and feasible approach to analyze the frequency characteristics of the singing phenomenon. Comparing the singing and nonsinging sound spectra of hydroacoustic signals, two abnormal peaks in a very narrow sound frequency interval can be observed in Fig. 2, which are the signals of vortex singing. In the case of vortex singing, the primary frequency near 488 Hz and its second harmonic signal can be observed with very large sound pressure levels, which are over 30 and 15 dB higher than in the nonsinging cases, respectively. Singing of a cavitating tip vortex can be observed at different incoming flow speeds in the present work. The tune of the singing shifts with the increment of the streamwise velocity W_∞ (see Fig. 3).

Using high-speed video images, we can extract detailed geometric information of the cavitating vortex in the singing state. Using edge detection and pixelation of the images, the cavity radius can be obtained using a toolbox in MATLAB. The spatial resolution is 0.14 mm per pixel. Temporal variations of the cavitating vortex radius are shown in Fig. 4. During the graphical postprocessing, 32 pixels are set to be the lowest threshold to capture the tip vortex cavity.

For the before-singing state, a temporal stable cavitating vortex tube is observed, as shown in Fig. 4(a). In contrast, the cavitating vortex tube in the singing state oscillates near the singing frequency according to the expansion and contraction of the vortex radius in Figs. 4(b) and 4(c). The nodes of the cavitating vortex tube [the green spots in Figs. 4(b) and 4(c)], e.g., $x = 15$ and 38 mm for $W_\infty = 7.0$ m/s, do not move temporally and spatially, indicating that the double helix mode remains unchanged, which implies that the singing cavity expands and contracts in phase and periodically.

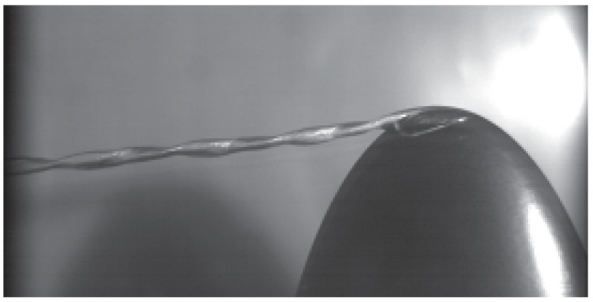

(a)

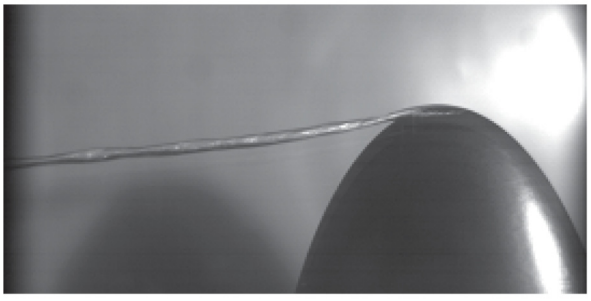

(b)

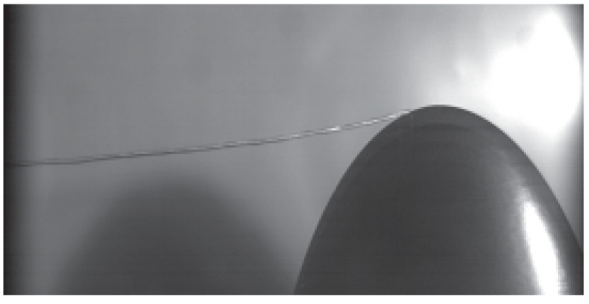

(c)

FIG. 1. Pictures from the high-speed camera at 2000 fps (a) before, (b) during, and (c) after vortex singing for $W_\infty = 12.8$ m/s, $\sigma = 1.40$, $\alpha/\alpha_s = 0.77$, and no nuclei seeding.

The deformation of the tip vortex can be divided into different modes according to the azimuthal wave number m [9,11]. The breathing mode $m = 0$, which is of physical importance, is associated with an alternation of high- and low-pressure perturbations. As indicated from the results of the high-speed photography, the breathing mode is speculated to be the main origin of the cavitating vortex singing. The second mode $m = 2$, or double helix mode, leads to an elliptical shape of the vortex core. From the high-speed video images, it is found that the breathing mode and double helix mode are the two dominant modes in the context of SCTV. Meanwhile, the tune shift, i.e., the singing frequency, can be observed clearly by comparing the temporal stripe widths in Figs. 4(b)

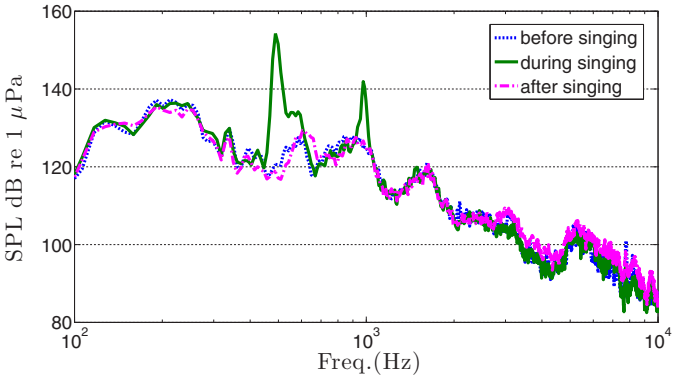

FIG. 2. Noise spectra of vortex cavitation before, during, and after vortex singing for $W_\infty = 12.8$ m/s and $\sigma_v = 1.40$.

and 4(c). Modes with larger azimuthal wave numbers m are found to be substantially damped due to viscosity [11] and are excluded in the following discussion.

The wavelength λ_z of the double helix vortex tube and the radius r_b of the cylindrical cavitating tip vortex tube can be obtained by a graphical postprocessing approach, as listed in Table I. For instance, we obtain $\lambda_z = 23$ mm from Fig. 4(a); therefore, the wave number $k_z = 2\pi/\lambda_z = 483\ \mathrm{m}^{-1}$.

III. LINEAR ANALYSIS OF THE RESONANCE FREQUENCY

A. Linear dispersion relationship

Ignoring viscous effects, the azimuthal velocity at the cavity interface is estimated using conservation of radial momentum or Bernoulli integration for the potential vortex flow [9],

$$V_c^p/W_\infty = \sqrt{2(p_\infty - p_v)/\rho W_\infty^2} = \sqrt{\sigma_v} \tag{1}$$

under the assumptions of axisymmetric flow conditions and zero radial velocity. Therefore, the azimuthal velocity can be calculated as long as the cavitation number σ_v and freestream velocity W_∞ are known. According to (1), the azimuthal velocity at the surface of the vortex tube is $V_c^p = \sqrt{\sigma_v} W_\infty \approx 1.2 W_\infty$ for the cases studied in Fig. 3 when $\sigma_v \approx 1.45$.

In the extended near field less than 10 times the chord length behind the hydrofoil, the tip vortex is in a state of roll-up and merging processes and is affected by the hydrofoil's boundary

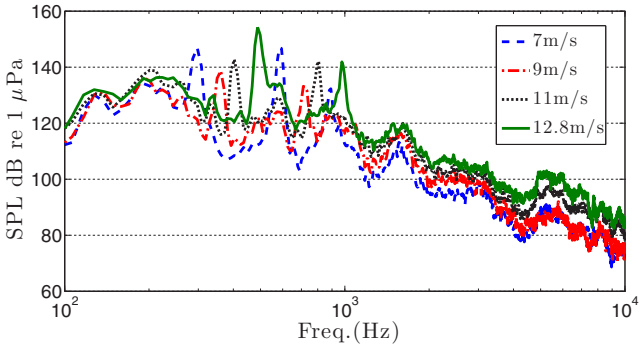

FIG. 3. Noise spectra of vortex singing for different flow velocities $W_\infty = 7$, 9, 11, and 12.8 m/s. The first frequency peaks are 297.2, 360.9, 403.4, and 488.3 Hz. Cavitation numbers σ_v are 1.45, 1.45, 1.45, and 1.40.

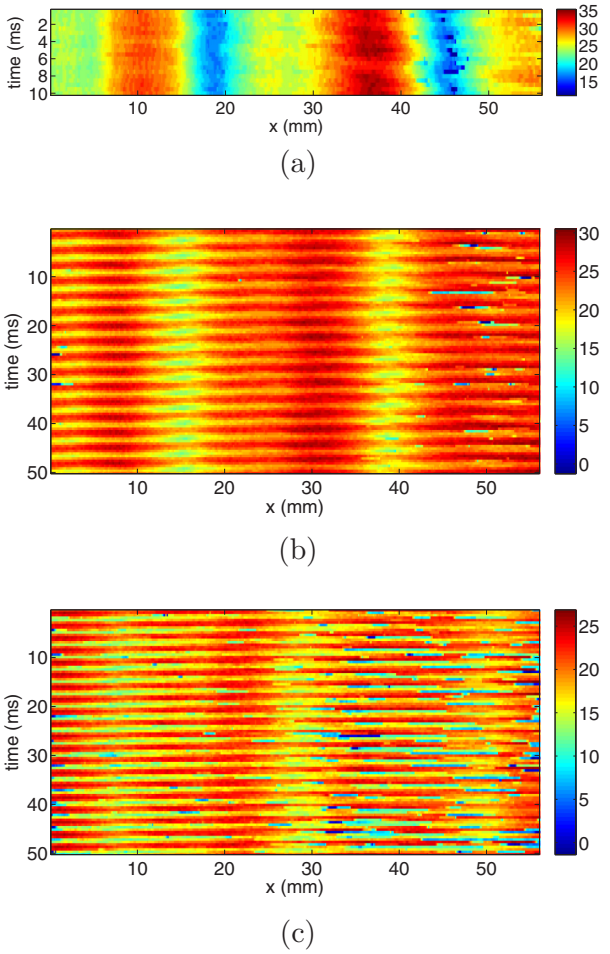

FIG. 4. Variation of the cavitating vortex radius in different flow states: (a) before singing for $W_\infty = 12.8$ m/s, (b) during singing for $W_\infty = 7.0$ m/s, and (c) during singing for $W_\infty = 12.8$ m/s. The coordinate origin $x = 0$ mm is the hydrofoil's tip.

layer wake [3]. When viscous effects are considered, classical two-parameter vortex models are not suitable for describing the cavitating tip vortex. The azimuthal velocity of the empirical cavitating vortex is smaller than that of the potential flow vortex. Based on experimental results, an empirical

TABLE I. Cavity geometry measured from the high-speed video.

W_∞ (m/s)	r_b (mm)
7.0	3.20
9.0	3.18
11.0	3.00
12.8	2.55

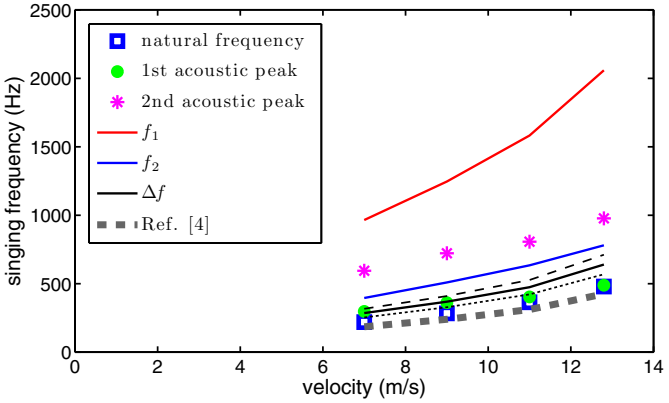

FIG. 5. Primary and second harmonics of singing waves versus incoming current speed W_∞ obtained by a hydrophone, as shown by open circles and stars, respectively. Red and blue lines represent the primary frequencies corresponding to f_1 and f_2. Black lines represent the modulation frequencies corresponding to $\Delta f = (f_1 - f_2)/2$: The solid line is the theoretical curve with the parameter $\beta = 0.40$, while the dashed and dotted lines are the results for $\beta = 0.45$ and 0.50, respectively.

cavitating vortex model has been proposed [12]. The azimuthal velocity at the cavity surface is

$$V_v^e|_{r_b} = \beta \frac{\Gamma}{2\pi r_b} = \beta V_c^p\big|_{r_b}, \tag{2}$$

in which the parameter β is defined as $\beta = \zeta r_b^2/(r_v^2 + \zeta r_b^2)$ with the constant $\zeta = 1.2564$. Early studies, employing the conservation of angular momentum, show that the cylindrical vapor bubble radius is $r_b = \sqrt{2} r_v$, relative to the initial core radius [13]. Typical values of β are as follows: For $r_b = r_v$, $\beta = 0.56$; for $r_b = 1.3 r_v$, $\beta = 0.40$; and for $r_b = 1.5 r_v$, $\beta = 0.33$. To determine the circulation $\Gamma = 2\pi r_b V_c^p|_{r_b}$, the mean radius of the cavitating vortex r_b is obtained from the high-speed video.

The dimensionless dispersion relationship presented by Pennings *et al.* [9] can be used to describe the kinematics of waves at the surface of the tip cavitating region

$$\frac{\omega_{1,2}}{W_\infty} = k_z + \frac{\beta\sqrt{\sigma_v}}{r_b}\left(n \pm \sqrt{\frac{-\kappa H_n'(\kappa)}{H_n(\kappa)}}\right), \tag{3}$$

where $\kappa = k_r r_b \approx i k_z r_b$. Clearly, it can be seen that the frequency ω depends linearly on the streamwise speed W_∞.

Using the linear dispersion relationship, the distributions of the surface wave frequency against the flow speed W_∞ are plotted in Fig. 5. For example, $W_\infty = 9$ m/s, $\sqrt{\sigma_v} \approx 1.2$, $r_b \approx 3.18$ mm, and $\lambda_z = 23$ mm. For $n = 2$ and $\kappa = k_r r_b = 0.7649i$, we require $\mathrm{Im}(k_r) > 0$ for finite values of $H_n(\kappa)$ when $r \to \infty$. In addition, $\sqrt{-\kappa H_2'(\kappa)/H_2(\kappa)} = 1.514$. However, neither the primary nor the second harmonics of the surface waves relates to the observed singing in the present work. The resonance of surface waves is unlikely to be the mechanism of SCTV.

B. Modulation of the surface waves

Now the problem is to determine what excites vortex singing since, as shown above, the resonance of surface waves is unlikely to be the mechanism. Let us consider the beat frequency of two superimposed wave components. Just around the hydrofoil tip, the secondary motions are most plausibly related to wake shedding, usually referred to as shape dilations or oscillations, which appears to provide the excitation source of the helical vortex structure [3]. The formation of highly concentrated and shedding vortices at the discontinuities of the hydrofoil tip acts as a wave maker.

Surface waves, following the intrinsic linear dispersion relationship, propagate along the cylindrical interface between the vapor cavity region and the liquid water region. To explain the beat frequency of two superimposed wave components, we may investigate the superposition of two equal-amplitude harmonic waves with frequencies $\omega_1 = \omega_0 + \Delta\omega$ and $\omega_2 = \omega_0 - \Delta\omega$,

$$e^{i[k_z z-(\omega_0+\Delta\omega)t]} + e^{i[k_z z-(\omega_0-\Delta\omega)t]} = 2e^{i(k_z z-\omega_0 t)} \cos \Delta\omega t, \tag{4}$$

in which

$$\Delta\omega r_b / W_\infty = \beta\sqrt{\sigma_v}\sqrt{-\kappa H_2'(\kappa)/H_2(\kappa)}, \tag{5}$$

according to formulation (3). The two downstream-going waves can result in a primary wave of frequency ω_0 modulated by a slower wave of angular frequency $\Delta\omega$. This kind of modulation $\cos \Delta\omega t$ is spatially stationary, in agreement with the observations in Fig. 4. For acoustic analysis in the frequency domain, we have $\Delta f = \Delta\omega/2\pi$.

The correlation between the singing frequency and the measured vapor core radius has been estimated with the empirical formulation $2\pi f r_b / W_\infty = 0.45\sqrt{\sigma_v}$ with $0.25 \leqslant 2\pi f r_b / W_\infty \leqslant 0.65$ [2,4], which is in the same form as the scaling law (5). As can be observed in Fig. 5, this empirical formulation is better than (5) in predicting the singing frequency. Therefore, it is important to know the physical meaning of the empirical parameters.

C. Natural frequency of the cavitating tip vortex

The natural frequency of the radial oscillation of a cylindrical bubble has been calculated analytically [14,15]. Under the assumption of axisymmetric and cylindrical flows, a two-dimensional Rayleigh-Plesset equation can be used to describe the motion of a cylindrical bubble, which corresponds to the mode $n = 0$ and $k_z = 0$. The oscillation period of a simple cylindrical bubble is estimated as

$$T_N = \frac{4\pi^2 r_b^2}{\Gamma}\sqrt{\ln\left(\frac{r_D}{r_b}\right)}, \tag{6}$$

which is plotted in Fig. 5. Because the experiments are conducted in a rectangular water tunnel, the half-width of the cross section is chosen as the value of $r_D = 125$ mm. Apparently, the ratio r_b/r_D is an important parameter for triggering the resonance. Singing of a cavitating tip vortex occurs only for tip vortex cavities of a particular radius.

Figure 5 clearly shows the correspondence between the intrinsic frequency of the radial oscillation of a cylindrical bubble and the first acoustic frequency of vortex singing. Considering Fig. 5 again, the possible resonance frequencies are compared for four cases with different streamwise velocities. The primary wave's two frequencies are not related to the natural resonance frequency f_N. However, it is shown that $\Delta f = (f_1 - f_2)/2 \approx f_N$, which implies that the modulation of the two primary waves of the helix mode may induce the subharmonic resonance.

It has been suggested that a form of periodic oscillation of a bubble driven at twice its resonance near a threshold might be emitted at subharmonic frequencies [16]. Surface waves on the bubble wall were one source of subharmonic generation [16]. Neppiras wrote the following: "Although it has never been found possible to relate subharmonic signals with surface-wave activity on the bubbles, surface waves would be expected to contribute to the $\nu/2$ signals [Δf in this paper]—the possibility is not yet ruled out" [17]. According to the comparison between the theoretical results and experimental data in the present work, the coincidence between the subharmonic resonance and the natural frequency appears to be the generation mechanism of SCTV. Physically, slowly increasing the background pressure varies the tip vortex radius in CSSRC water tunnel experiments. When the size of the cavitating tip vortex meets the resonance criterion, the singing of the tip vortex occurs.

To further verify the proposed generation mechanism of SCTV, we investigate the phenomenon under different flow regimes using experimental data from different facilities. Equation (6) could be

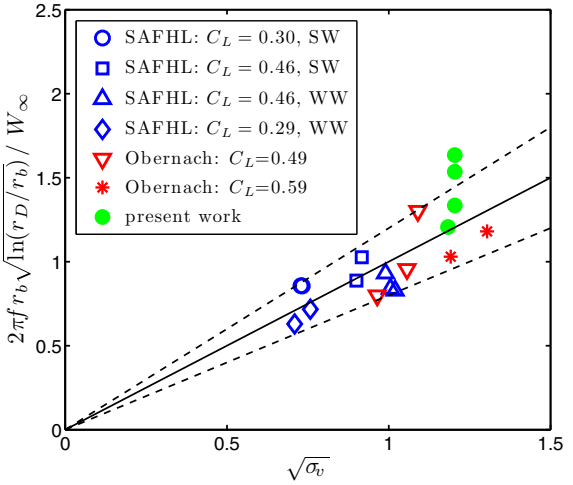

FIG. 6. Comparison among experimental data and the analytical formulation. The solid line is the analytical formulation (7), while dashed lines are ±20% off the exact formulation. Other experimental data are read from [4]. Here SW represents strong water and WW represents weak water.

rewritten as

$$\frac{2\pi f r_b}{W_\infty} = \frac{\sqrt{\sigma_v}}{\sqrt{\ln(r_D/r_b)}}, \tag{7}$$

which is the final formulation we obtained to predict the frequency of SCTV. Three sets of experimental data are compared against the theoretical formulation (7) in Fig. 6. To clarify the early experimental conditions, we read the experimental data, including the SCTV diameter, frequency, streamwise velocity, and cavitation number when singing occurs, from Figs. 5, 6, and 8 in Ref. [4]. Half cross-section widths $r_D = 95$ and 150 mm are used as the characteristic water tunnel sizes for St. Anthony Falls Hydraulic Laboratory (SAFHL) and Versuchsanstalt für Wasserbau in Obernach, respectively. These experimental data cover a large range of flow parameters: The core size of SCTV r_b varies between 0.4 and 3.5 mm, cavitation number σ_v varies between 0.53 and 1.70, and the singing frequency varies between 300 and 1600 Hz approximately. Good agreement is obtained between the theoretical formulation and experimental data as shown in Fig. 6.

As mentioned in the early studies [4], the SAFHL data have the same trend as the Obnernach data, but the trend is followed in steps rather than linearly. Taking the water tunnel size into account, the experimental data obtained in all experimental facilities coincide well with the new scaling law, as shown in Fig. 6, which implies that Eq. (7) reflects the physical process of SCTV.

IV. CONCLUSION

Extensive experimental investigation and analysis of SCTV for the elliptic hydrofoil with section NACA 66_2-415 were carried out in this paper. As a summary, the generation mechanism of SCTV is one kind of resonance at the natural frequency, proposed in Sec. III C of the present work, which is totally different from the modulation of surface waves as suggested in previous studies. Singing of a cavitating tip vortex may emit acoustic signals at both the primary frequency and higher-order harmonics, which is a typical characteristic of resonance in many physical processes. Vortex singing only exists in the transition process between strong tip vortex cavitation and weak tip vortex cavitation. Supported by the experimental results, surface wave activity on the bubbles is speculated to be the exciting source of the subharmonic emission.

ACKNOWLEDGMENTS

X.P. would like to acknowledge Dr. Arndt for his lectures at CSSRC, which stimulated the interest in SCTV. Professor van Terwisga and Dr. Pennings from MARIN provided the hydrofoil profile studied in present work. Support from the National Natural Science Foundation of China (Grants No.11332009 and No.11272210) is greatly appreciated.

---

[1] R. E. A. Arndt, V. Arakeri, and H. Higuchi, Some observations of tip-vortex cavitation, J. Fluid Mech. **229**, 269 (1991).
[2] R. Arndt, Cavitation in vortical flows, Annu. Rev. Fluid Mech. **34**, 143 (2002).
[3] C. Breitsamter, Wake vortex characteristics of transport aircraft, Prog. Aerosp. Sci. **47**, 89 (2011).
[4] B. Maines and R. E. A. Arndt, The case of the singing vortex, J. Fluids Eng. **119**, 271 (1997).
[5] H. Higuchi, R. E. A. Arndt, and M. Rogers, Characteristics of tip vortex cavitation noise, Trans. ASME J. Fluid Eng. **111**, 495 (1989).
[6] L. Briançon-Marjollet and L. Merle, *Proceedings of the 21st Symposium on Naval Hydrodynamics* (National Academy, Washington, DC, 1997).
[7] A. Binnie, Annular Borda flow, J. Fluid Mech. **19**, 187 (1964).
[8] J. Keller and M. Escudier, Theory and observations of waves on hollow-core vortices, J. Fluid Mech. **99**, 495 (1980).
[9] P. Pennings, J. Bosschers, J. Westerweel, and T. van Terwisga, Dynamics of isolated vortex cavitation, J. Fluid Mech. **778**, 288 (2015).
[10] See Supplemental Material at http://link.aps.org/supplemental/10.1103/PhysRevFluids.2.053602 for acoustic recordings.
[11] D. Fabre, D. Sipp, and L. Jacquin, Kelvin waves and the singular modes of the Lamb-Oseen vortex, J. Fluid Mech. **551**, 235 (2006).
[12] P. Pennings, J. Westerweel, and T. van Terwisga, Flow field measurement around vortex cavitation, Exp. Fluids **56**, 206 (2015).
[13] R. E. A. Arndt and A. Keller, Water quality effects on cavitation inception in a trailing vortex, J. Fluids Eng. **114**, 430 (1992).
[14] T. Leighton, *The Acoustic Bubble* (Academic, New York, 1997).
[15] J. Choi, C. Hsiao, G. Chahine, and S. Ceccio, Growth, oscillation and collapse of vortex cavitation bubbles, J. Fluid Mech. **624**, 255 (2009).
[16] E. Neppiras, Acoustic cavitation, Phys. Rep. **61**, 159 (1980).
[17] E. Neppiras, Subharmonic and other low-frequency emission from bubbles in sound-irradiated liquids, J. Acoust. Soc. Am. **46**, 587 (1969).